Effect of Carbon Coating on the Properties and Electrochemical Performance of LiFePO₄/C Composites by Vacuum Decomposition Method

Xiaopeng Huang[1,2,3], Yuanchao Du[1,2], Pengwei Qu[1,2,3], Feng Liang[1,2,3], Yongnian Dai[1,2,3] and Yaochun Yao[1,2,3,]*

[1] Faculty of Metallurgical and Energy Engineering, Kunming University of Science and Technology, Kunming 650093, China
[2] Engineering Laboratory for Advanced Batteries and Materials of Yunnan Province, Kunming University of Science and Technology, Kunming 650093, China
[3] National Engineering Laboratory for Vacuum Metallurgy, Kunming 650093, China
[*]E-mail: yaochun9796@163.com

A modified method of carbon coating by vacuum decomposition was employed to synthesize nano-sized LiFePO₄/C cathode material. Sucrose, polyvinyl alcohol (PVA) and citric acid (CA) were used as different carbon resource and their pyrolysis behavior on the properties of the LiFePO₄/C composite was also investigated. During vacuum decomposition process, the organic carbon suppressed particle growth and decreased particle agglomeration, resulting in homogeneous carbon coated material. Among them, the sucrose coated LiFePO₄/C sample exhibited reduced particle size, regular spherical grains and graphitized carbon coating, indicating an enhancement to electrochemical performance. The sample delivered high specific capacity of 123.9 mAh/g at 5C and good capacity retention of 96.2% after 100 cycles at 1C. A comparison of carbon coating by traditional argon atmosphere and vacuum condition further demonstrated that vacuum decomposition method is conducive to refining particle for better carbon coating, leading to dramatically improved electrode polarization and rate performance of LiFePO₄/C composite.

1. INTRODUCTION

In recent years, there has been a dramatic demand of rechargeable lithium-ion batteries (LIBs) with low cost, high-performance and high safety for electric and plug-in electric vehicles [1, 2]. In

LIBs, the cathode materials play an important role in the determination of battery energy density, life cycle, safety and cost. Among them, olivine-type $LiFePO_4$, first introduced by Padhi *et al*, has attracted great interest in terms of its high theoretical capacity (170 mAh/g), good cycle stability, low cost and safety [3]. For practical application of pristine $LiFePO_4$, one of the main obstacles is its poor rate performance, which can be ascribed to poor electric conductivity ($\sim 10^{-8}$ to 10^{-10} S/cm) and sluggish Li^+ ion diffusion ($\sim 10^{-18}$ cm^2/s) [4]. At present, many approaches have been applied to modify the material, such as conductive surface coating [5-7], size reduction [8-10] and ions doping [11-13]. Compared to other methods, carbon coating is the most common way to improve the property of $LiFePO_4$. It is well known that the morphology and electrochemical performance of $LiFePO_4$/C markedly depends on carbon sources, carbon content and thickness, carbon structure and distribution [14].

Usually, carbon coated $LiFePO_4$/C composite is synthesized via solid-state reaction [5], hydrothermal process [7], sol-gel method [15] and spray-drying technique [16]. Solid-state reaction method, which involves the blending of ingredients by ball-milling followed by thermal treatment at high temperature, has turned out to be a versatile technique for scale up. However, it needs high reaction temperatures, long reaction time and, especially, protective atmosphere (N_2 or Ar) to generate a pure phase and well-ordered structure of $LiFePO_4$/C composite. An alternative technique, vacuum sintering, has been proposed to synthesize cathode materials for high efficiency and energy conservation. Vacuum sintering is widely used for material calcination at a pressure condition of medium vacuum (1333–1.33×10^{-1} Pa), high vacuum (1.33×10^{-1}–10^{-6} Pa), or even ultra-high vacuum ($<10^{-6}$ Pa). When using solid-state reaction method to prepare $LiFePO_4$, the decomposition of precursor usually involves the exhaust of gaseous products, such as CO_2, CO, NH_3, and H_2O. Therefore, vacuum sintering is a suitable method for not only accelerating the decomposition reaction but decreasing extra inert/reductive gas consumption. The $LiFePO_4$/C composite has been successfully synthesized under vacuum condition in some reports [17-21]. For example, Huang *et al.* have studied the effect of different lithium source (Li_2CO_3 and LiOH) on the properties of $LiFePO_4$/C under vacuum condition, showing a higher discharge capacity with smaller particles by using LiOH as lithium salt. Guo *et al.* have prepared two kinds of $LiFePO_4$/C from direct solid-phase synthesis and vapor deposition respectively, and the latter exhibited good structure and excellent electrochemical performance. Zhang *et al.* successfully synthesized $LiFePO_4$/C via a two-step vacuum sintering method, which showed better performance than $LiFePO_4$ without carbon coating. In our previous work, porous $LiFePO_4$/C composite was obtained by one-step vacuum sintering, and the sintering time and temperature of vacuum sintering for preparation have been studied [22]. However, problems remain in optimizing the preparation parameters of vacuum sintering, such as the degree of vacuum, carbon sources, carbon content and so on.

In this work, we report a modified method to prepare carbon coated $LiFePO_4$/C composite by vacuum decomposition process. Owing to the free of gas and pressure under vacuum condition, the purity, structure and morphology of obtained material may change unexpectedly. Three common sources of carbon, sucrose, polyvinyl alcohol (PVA) and citric acid (CA) were chosen to cover on the $LiFePO_4$ particle. The microstructure, distribution as well as content of coating carbon on the particle surface has been investigated. The relationship of carbon sources and electrochemical performance of $LiFePO_4$/C composite is intensively studied. Besides, a sucrose coated $LiFePO_4$/C composite

synthesized under traditional argon atmosphere (101325 Pa) was performed for comparison. The sphere-like and well-dispersed LiFePO$_4$/C nanoparticles exhibit superior rate and cycling performance, which benefits from the effective carbon coating and fast Li$^+$ ions diffusion rate by vacuum decomposition method.

2. EXPERIMENTAL PROCEDURE

2.1 Synthesis

As show in Fig. 1, carbon coated LiFePO$_4$/C material was synthesized by a two-step solid state reaction with vacuum decomposition process. First, stoichiometric amounts of Li$_2$CO$_3$ (AR), FeC$_2$O$_4$·2H$_2$O (AR), NH$_4$H$_2$PO$_4$ (AR) were ball milled together using ethanol as disperser for mechanochemical activation. Then the resulting slurry was dried and pre-calcination at 350 ℃ for 4 h under Ar atmosphere protection. After decomposition of precursor and expelling of gasses, the gray LiFePO$_4$ (named as LFP) was obtained.

To investigate the effect of carbon coating on LiFePO$_4$ under vacuum sintering condition, sucrose, PVA and CA was separately added and acted as the carbon source. For instance, the as-prepared LiFePO$_4$ powder was reground with 7 wt.% sucrose and sintered in a vacuum tube furnace. Before sintering, the furnace was evacuated firstly, and then argon was injected into the chamber, this was repeated three times to ensure the evacuation of oxygen. The vacuum condition was maintained at a pressure of about 10~1 Pa by operating a vacuum pump during sintering. In this case, the sucrose can rapidly fuse and disintegrate in advance for a better coating. Finally, LiFePO$_4$/C sample was obtained by sintered the ground powder at 650 ℃ for 6 h under vacuum condition. Similarly, the 7 wt.% PVA coated LiFePO$_4$/C and the 7 wt.% CA coated LiFePO$_4$/C samples were synthesized by the same route. The LiFePO$_4$/C samples with different carbon coating by sucrose, PVA and CA were designated as LFP/C-1, LFP/C-2 and LFP/C-3, respectively. For comparison, 7 wt.% sucrose coated LiFePO$_4$/C sample (named as LFP-4) was prepared by calcining the powder under traditional Ar atmosphere protection.
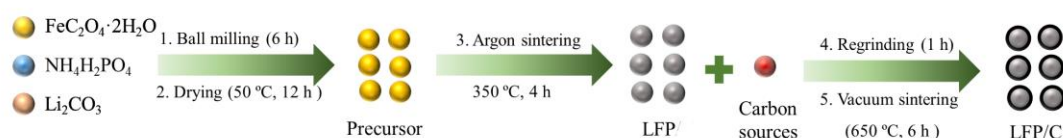
Figure 1. Preparation procedure of carbon coated LiFePO$_4$/C via vacuum decomposition method.

2.2 Materials characterization

The crystal structures of the obtained samples were determined by X-ray diffraction (XRD, D/Mac-3c, Rigaku) equipped Cu kα radiation. The morphological observation was carried out by scanning electron microscopy (SEM, S4800, Hitachi) and field-emission transmission electron

microscopy (TEM, Tecnai-TF30, FEI). Surface analysis was operated utilizing Raman spectroscopy (Renishaw, inVia) and the data was fitted by peakfit 4.12 software (Seasolve software Inc.). The carbon content in $LiFePO_4/C$ composites was characterized with infrared carbon-sulfur analyzer (Corey-230B, Kerui).

2.3 Electrochemical characterization

Electrochemical measurements were performed by using the CR2025 coin-type cell with metallic lithium foil as the negative electrode and Celgard 2400 microporous membrane as the separator. The working electrode was prepared by mixing 80 wt.% of active material with 10 wt.% of acetylene black as a conductive reagent and 10 wt.% of polyvinylidene fluoride (PVDF) dissolved in N-methyl pyrrolidinone (NMP) as a binder. Then the slurry was uniformly coated onto an aluminum current collector, and further dried at 80 ℃ under vacuum for 24 h. The dried electrode was cut into wafer with the diameter of 13.5 mm. And then, the cells were assembled in a glove box filled with Ar gas using an electrolyte composed of 1 mol/L $LiPF_6$ in ethylene carbonate and diethyl carbonate (EC/DEC, 1:1 in volume). Galvanostatic charge-discharge cycling test was carried out on an electrochemical test instrument (Qingtian, KTBS93, China) at various current densities between 2.0 and 4.2 V *vs*. Li/Li^+ at room temperature (25 ℃). Electrochemical impedance spectroscopy (EIS) was performed by an electrochemical workstation (Chenhua, CHI600E, China), in the frequency range of 1 MHz to with an applied perturbation signal of 10 mV.

3. RESULTS AND DISCUSSION

3.1 structure and morphology analysis

XRD patterns of the different samples under study are shown in Fig. 2. The peak of the $LiFePO_4$ (LFP) sample obtained at 350 ℃ can be well indexed to orthorhombic olivine structure belonged to Pnmb space group (JCPDS NO.40-1499). After subsequent heat treatment and carbon coating under vacuum condition, the resulted $LiFePO_4/C$ composites show stronger and narrower diffraction peaks than pure $LiFePO_4$, meaning a perfect crystallinity is obtained. There is no evidence of diffraction peaks related to carbon, indicating that the carbon decomposed from organics was amorphous. The content of residual carbon for LFP/C-1, LFP/C-2 and LFP/C-3 was about 3.1%, 2.5% and 2.2%, respectively, determined by carbon-sulfur analyzer. Table 1 lists the lattice parameters and the crystal size of obtained samples after cell refinement, where the crystal size is calculated by Scherer formula: $D=k\lambda/(\beta cos\theta)$ (k is 0.9, λ is 0.15406 nm for Cu $k\alpha_1$ radiation and β is the FWHM of the diffraction peak on a 2θ scale, respectively [23]). The lattice parameters are generally considered as a measure of the Li/Fe cation disorder in the as-prepared $LiFePO_4$ phase [24]. It can be seen that the lattice parameters of $LiFePO_4/C$ after vacuum sintering closes to the theoretical values (No. 40-1499) than that of pure $LiFePO_4$, further indicating the complete crystallization and order of Li/Fe cation. Analysis of crystal size calculated using D_{131} diffraction peak reveals that the pyrolytic sucrose is conducive to suppressing grain growth in the following heating treatment process.
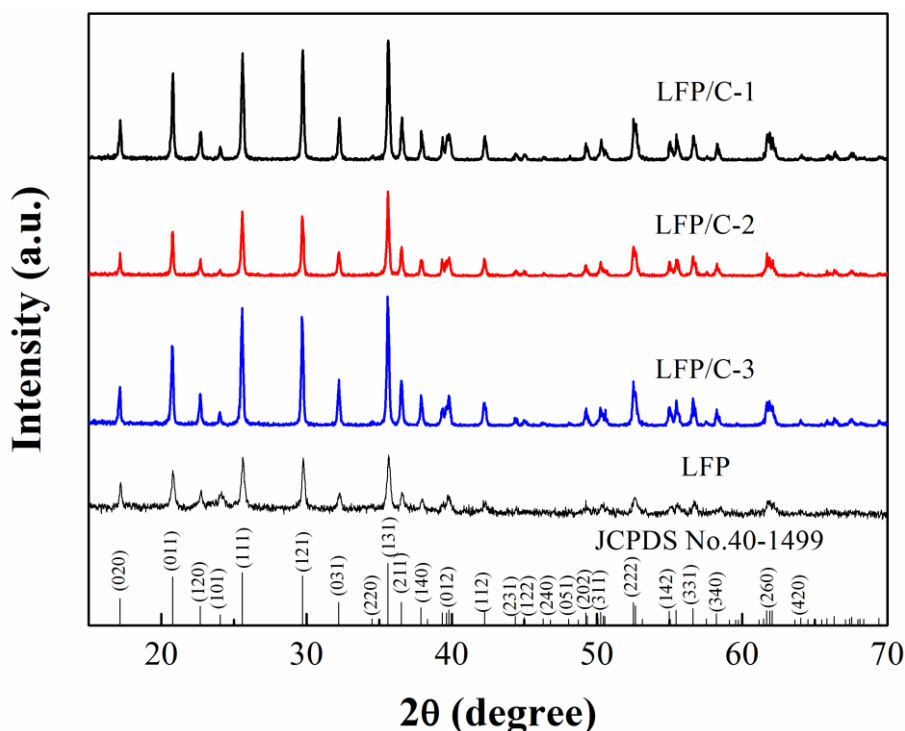
Figure 2. XRD patterns of LiFePO$_4$ and carbon coated LiFePO$_4$/C by different carbon sources.

Table 1. The lattice parameters and crystal size ofthe synthesized LiFePO$_4$ and LiFePO$_4$/C samples.

Sample	Lattice parameters				Crystal size (D$_{131}$) /nm
	a /nm	b /nm	c /nm	V /nm^3	
LFP	1.031	0.598	0.467	287.92	40
LFP/C-1	1.032	0.601	0.469	290.89	58
LFP/C-2	1.033	0.601	0.470	291.80	79
LFP/C-3	1.031	0.600	0.469	290.12	90
No.40-1499	1.033	0.601	0.469	291.17	-----

Fig. 3 illustrates the morphological characterisation of pure LiFePO$_4$ and LiFePO$_4$/C composites analyzed by SEM. The precalcined sample LiFePO$_4$ (Fig. 2a) showed aggregated nanosize particles with irregular in shape, indicating solid state reaction is insufficient at low temperature. After calcination treatment of 650 ℃ and decomposition of carbon under vacuum, the microstructure of the LFP/C-1(Fig. 2b) turned to well-defined spherical particle with uniformly distributed and homogeneous in size, whereas the particle size became larger for LFP/C-2 (Fig. 2c) and particle shape showed irregular for LFP/C-3 (Fig. 2d). The average particle size of LFP/C-1, LFP/C-2 and LFP/C-3 was detected as ~60–200 nm, ~80–350 nm and ~90–400 nm, respectively. Among the samples, LFP/C-1 showed a smaller particle size and more intimate particle connection after carbon coating, suggesting the shorter distance for Li-ion diffusion. It is noting that the closer of particles may cause

some agglomeration for LFP/C-1 sample, which may be unfavorable for the penetration of electrolyte. Many researches have showed that carbon coating can suppress particle growth and decrease particle agglomeration [25, 26].
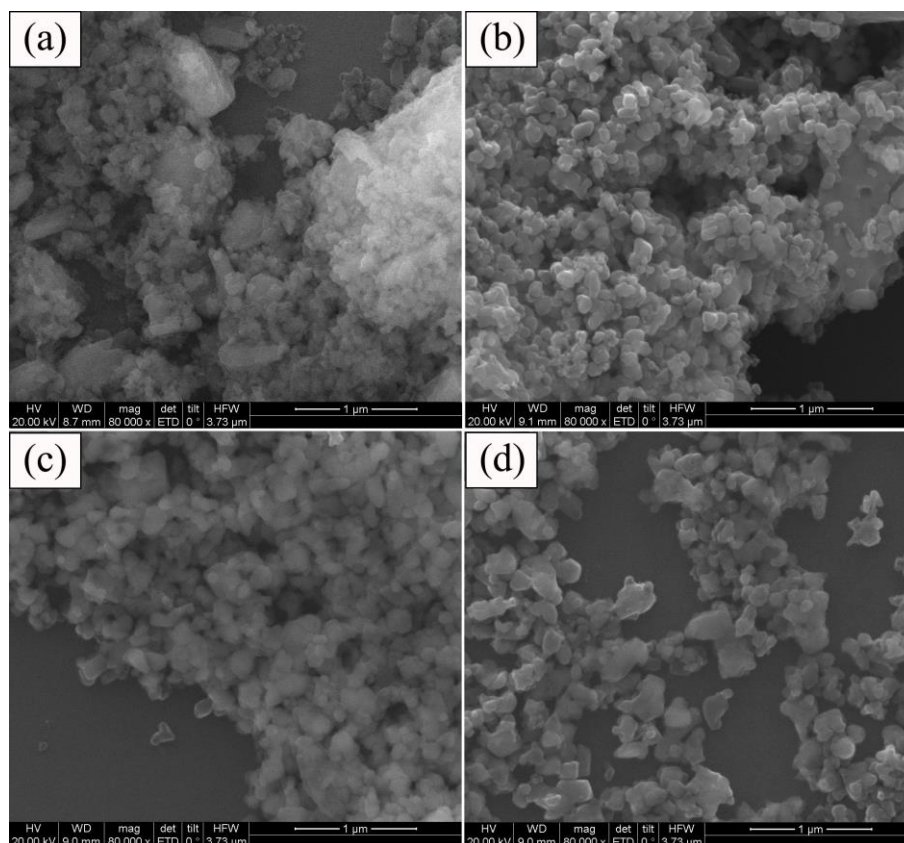
Figure 3. SEM images of LiFePO$_4$ and carbon coated LiFePO$_4$/C samples: (a) LFP, (b) LFP/C-1, (c) LFP/C-2 and (d) LFP/C-3.

Moreover, the choice of appropriate carbon precursors could directly affect the carbon structure, carbon content and carbon thickness of the composite. For example, the particles of LiFePO$_4$/C composite appeared rough surface when using sucrose as carbon source, resulting in increased specific surface area [7]. By PVA carbon coating, hollow structure of C-LiFePO$_4$ powder consisted of agglomerate particles was synthesized, which favored the penetrating and soakage between cathode material and electrolyte [25]. The sponge-like porous particles of LiFePO$_4$/C composite can be obtained after the pyrolysis of CA during the decomposition process [26]. In this study, different particles morphology was observed for carbon coated LiFePO$_4$/C on the basis of SEM analysis. The reasons can be explained by the decomposition and carbonization of organic material operated in vacuum condition (10~1 Pa) rather than traditional inert or reducing atmosphere (~101325 Pa). It can be seen that resources of carbon also played an important role on the crystallization and particle growth due to their different pyrolysis process. As a consequence, a suitable carbon source is essential to prepare a rounded shape, well-dispersed and uniform carbon coated LiFePO$_4$ by vacuum decomposition method.
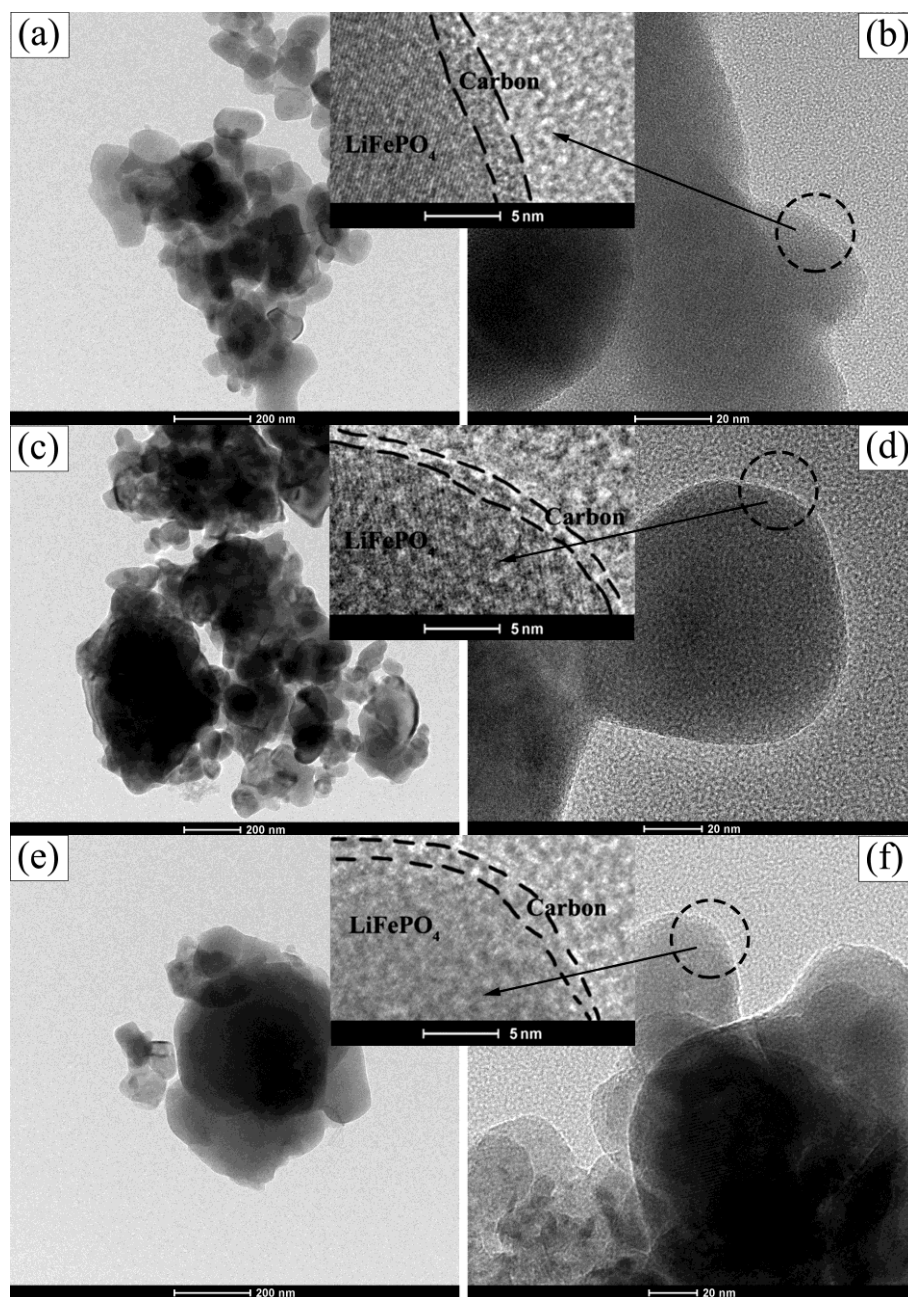
Figure 4. TEM images of carbon coated LiFePO$_4$/C samples: (a, b) LFP/C-1, (c, d) LFP/C-2 and (e, f) LFP/C-3 (the insets are magnifying images).

Fig. 4 exhibits the TEM image of LiFePO$_4$/C samples coated by different carbon sources. The size of primary particle varied according to carbon sources. For the LFP/C-1 (Fig. 4a and b), the smaller and uniform primary particle was obtained, and its surface is covered by amorphous carbon about 2-3 nm, resulting in fast electrode kinetics. Whereas, the LFP/C-2 (Fig. 4c and d) and LFP/C-3 (Fig. 4e and f) showed large particle size, uneven particle shape and thin carbon coating, indicating its poor electronic conductivity. The TEM result is in good agreement with the XRD and SEM analysis above, which suggests the source of carbon plays a crucial role in the structure and morphology of LiFePO$_4$/C composite after vacuum decomposition.
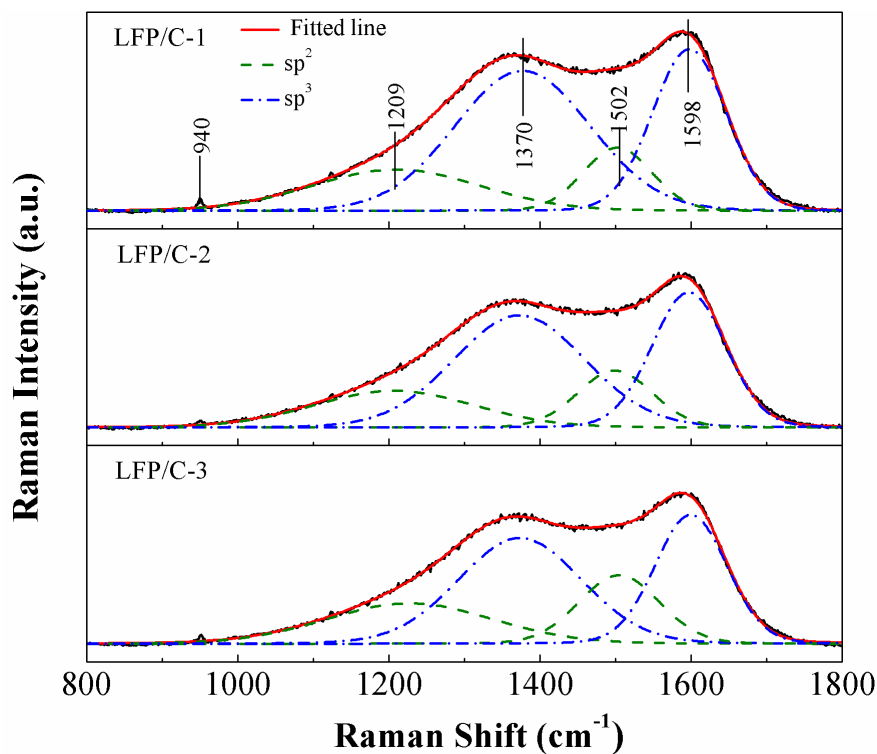
Figure 5. Raman spectra in the 800-1800 cm^{-1} region of carbon coated LiFePO$_4$/C samples.

To further characterize the surface structure of the as-prepared LiFePO$_4$/C samples, Raman spectra are collected and shown in Fig. 5. All Raman spectra consist of a relatively small band at ~940 cm^{-1}, which corresponds to the symmetric PO$_4^{3-}$ stretching vibration of LFP, and two broad peaks at about 1370 and 1598 cm^{-1} can be attributed to the D band and the G band of residual carbon, respectively [27]. The D band is due to the presence of defect and disorder in the graphitized carbon, while the G band corresponds to the E$_{2g}$ vibration mode of the ordered graphitized carbon [28]. The relative intensity of D and G bands can be a useful index for comparing the degree of crystallinity of various carbon materials. The position of the G band shifts downward to ~1500 cm^{-1} for amorphous carbon, when a loss of aromatic bonding appears [29]. Thus, a deconvolution using four Gaussian bans is used to account for the observed Raman features. The spectra is fitted with four components, the maximum of which appear at 1209, 1370, 1502 and 1598 cm^{-1}, respectively. The intensity of these two bands I$_D$ and I$_G$ is defined as the integral of these two Gaussians. It can be calculated that the *I$_D$/I$_G$* value of LFP/C-1, LFP/C-2 and LFP/C-3 composite was 0.85, 0.83 and 0.82, respectively. These are actually smaller than the value of ~1.0 in the traditional solid state route or other synthesis methods [30-32]. This change may be attributed to the increasing amount of carbon decomposed into ordered graphitized carbon under high vacuum condition, where the required transformation temperature is lower. A smaller *I$_D$/I$_G$* value indicates a higher degree of ordered graphitized carbon in the materials, resulting in better conductivity. Furthermore, the bands at ~1370 cm^{-1} (D band) and 1598 cm^{-1} (G band) are assigned to sp^2-type graphite structure and the other two band at ~1209 and 1502 cm^{-1} are attributed to tetrahedral sp^3-like disordered carbon with smaller conductivity [28]. The ratio of sp^2/sp^3 value of LFP/C-1, LFP/C-2 and LFP/C-3 composite was 2.75, 2.43 and 1.81, respectively. Swain *et al.* pointed

out that the electrochemical properties were found to be better in samples with large sp^2 bonder carbon [33]. Note that the difference of I_D/I_G value for the three samples is less than 3%, the superior of the sample judged by sp^2/sp^3 value is obviously more convincing. Consequently, the LFP/C-1 sample with a low I_D/I_G ratio (0.85) and a higher sp^2/sp^3 ratio (2.75) is believed to show a better conductivity for enhanced electrochemical performance.

3.2 Electrochemical properties
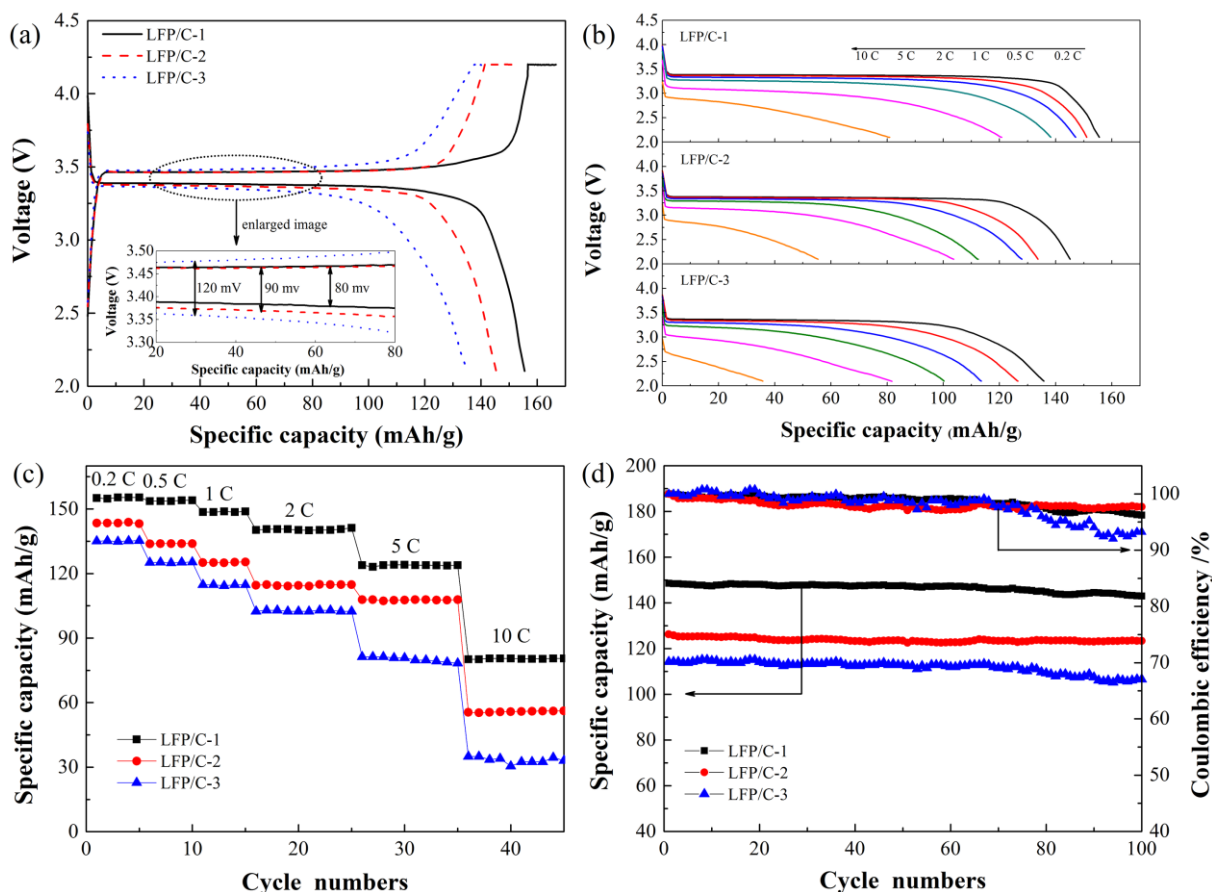
Figure 6. (a) The initial charge-discharge profiles for the LiFePO$_4$/C electrodes at 0.2C (the inset shows a magnification of the flat regions). (b) Discharge curves for the samples at different rate (from 0.2C to 10C). (c) Rate performance of the obtained samples from 0.2C to 10C. (d) Cycling performance of prepared samples at 1C.

Fig. 6 shows the electrochemical performance of LiFePO$_4$/C composite coated by different carbon sources. As shown in Fig. 6a, the charge-discharge profiles of the LFP/C-1, LFP/C-3 and LFP/C-3 samples at 0.2C are compared. Typical flat plateaus over the voltage range of ~3.4-3.5 V were obtained for all samples. Compared with LFP/C-2 and LFP/C-3, LFP/C-1 showed higher charge and discharge capacities and lower potential interval, while the other samples suffered from a large polarization loss. The polarization between the charge and discharge plateau of the samples is measured in the enlarged image. The potential interval was 80, 90 and 120 mV for LFP/C-1, LFP/C-2 and LFP/C-3 electrode, respectively. All of this improvement can be attributed to the fact that LFP/C-1

had smaller particles size and better carbon coating which is beneficial for Li-ion and electron migration. Furthermore, a comparison of the discharge profiles of the samples at different rates is displayed in Fig. 6b. It can be seen that the LFP/C-1 composite showed the best performance from 0.2C to 10C, revealing that smaller particle size and homogeneous carbon coating with high sp^2/sp^3 ratio can substantially improve the high rate capacity of $LiFePO_4$/C cathode material.

Fig. 6c presents the discharge capacity as a function of cycle number for the obtained samples at different current rates during the voltage range of 2.0-4.2 V. In comparison to LFP/C-2 and LFP/C-3, the LFP/C-1 delivered higher specific discharge capacities of 155.1 mAh/g, 153.7 mAh/g, 148.6 mAh/g, 140.3 mAh/g, 123.9 mAh/g and 80.1 mAh/g from 0.2C to 10C, respectively. The high capacity and low potential interval of the LFP/C-1 cathode are believed to be related to the spherical-like particles and better carbon structure. In addition, the as-prepared $LiFePO_4$/C cathode also displayed satisfactory cycling stability, as shown in Fig. 6d. After 100 cycles at 1C, the LFP/C-1, LFP/C-2 and LFP/C-3 cathode still retained 96.2%, 97.7% and 93.2% of its initial capacity, respectively. A relatively low coulombic efficiency (96.2%) was observed for LFP/C-1, which might be ascribed to the agglomeration of inner particle that unfavorable for the penetration of electrolyte after long term charge-discharge cycles.
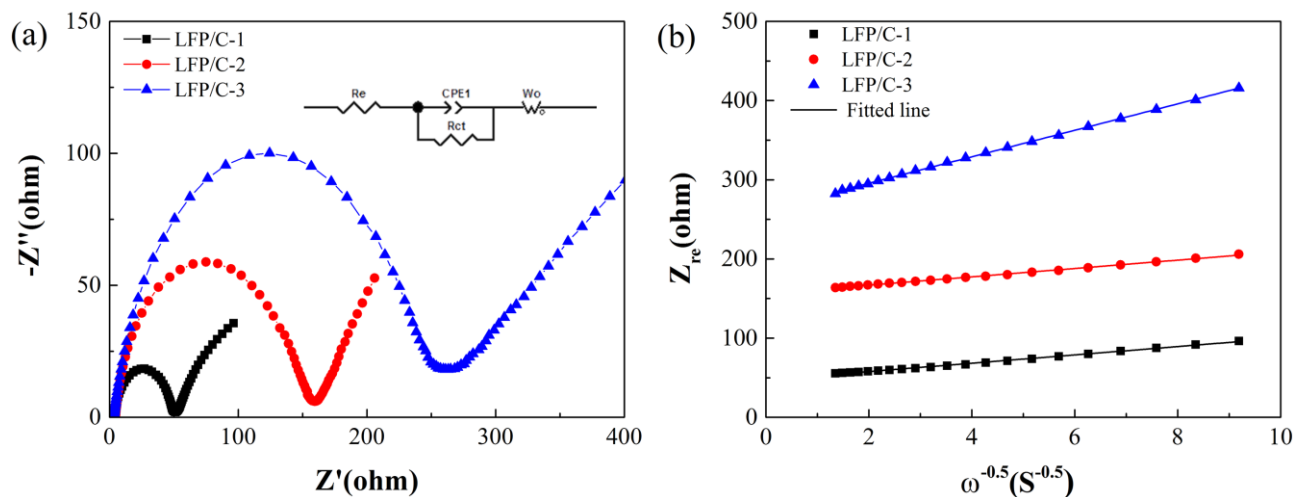
Figure 7. (a) Nyquist plots of $LiFePO_4$/C electrodes with a frequency range from 0.01 Hz to 100 KHz (the inset is the equivalent circuit). (b) The relationship between Z_{re} and $\omega^{-0.5}$ at low frequency (the continuous lines are fitted data).

Fig. 7 shows the EIS measurements of $LiFePO_4$/C coated by different carbon resources. All the Nyquist plots (Fig. 7a) are composed of two partially overlapped semicircles in the medium frequency regions and a straight line in the low frequency regions. The intercept in the high frequency region of the Z' real axis corresponds to the electrolyte solution resistance (R_e) of cell, the semicircle refers to the charge transfer resistance (R_{ct}) in the LFP/C cathode-electrolyte interface, and the slope line corresponds to Li^+ ion diffusion into the bulk electrode material (W_o) [34]. An equivalent circuit using symbols of R_e, R_{ct}, CPE_1 and W_o is fitted for the electrochemical impedance spectra data. The derived impedance parameter R_{ct} of LFP/C-1, LFP/C-2 and LFP/C-3 was 48.67, 151.16 and 229.23 Ω,

respectively. The smallest R_{ct} of LFP/C-1 sample indicates a decrease of charge transfer polarization resistance, which is obviously conductive to improving electrochemical performance. The apparent chemical diffusion coefficient of Li^+ ions can be calculated using the following equations [35]:

$$D = \left(R^2 T^2\right) / \left(2A^2 n^4 F^4 \sigma^2 C^2\right) \qquad (1)$$

$$Z_{re} = R_e + R_{ct} + \sigma \omega^{-0.5} \qquad (2)$$

Where R is the gas constant (8.314 J/(mol K)), T is the absolute temperature (298.15 K), F is Faraday's constant (96500 C/mol), A is the area of the electrode surface (1.43 cm^2), n is the number of electrons per molecule during oxidation, C is the concentration of Li^+ ions (0.01 mol/cm^3), σ is the Warburg factor, and ω is the angular frequency in the low frequency region. The plots of Z´ vs. $\omega^{-0.5}$ of LiFePO$_4$/C electrode are shown in Fig. 7b. According to the above equation, the Li^+ ions diffusion coefficient of LFP/C-1, LFP/C-2 and LFP/C-3 was 7.24×10^{-12}, 7.22×10^{-12} and 7.17×10^{-13} cm^2/s, respectively, which are similar to the previous reported values for LiFePO$_4$/C composite [36, 37]. It can be seen that the D_{Li}^+ value for LFP/C-1 or LFP/C-2 is an order of magnitude higher than the LFP/C-3, which can be attributed to shorter Li-ion diffusion distance. That is to say, the smaller particle size and regular shape play positive roles on the chemical diffusion coefficient of cathode material.

3.3 Comparison with argon atmosphere condition

Fig. 8 shows the comparison of sucrose coated LiFePO$_4$/C composite synthesized under vacuum condition and traditional argon atmosphere. For sample LFP/C-1 (Fig. 8a), uniform and well-dispersed particle can be found, while the LFP/C-4 (Fig. 8b) possesses irregular morphology with poor size distribution and serious agglomeration, indicating the uncontrollable particle growth and agglomeration under traditional argon sintering atmosphere. The residual carbon amount of LFP/C-1 and LFP/C-4 was 3.1% and 5.5%, which demonstrates that the vacuum condition can accelerate the pyrolysis of organic carbon leading to a lower residual content. It can be assumed that the unsatisfied morphology of LFP/C-4 may lead to uneven carbon coating for inferior conductivity. Thus, shorter plateau and longer sloping region is observed in the charge-discharge curves of LFP/C-4 sample when compared with LFP/C-1 sample (Fig. 8c). The terrible particle morphology and large polarization apparently affects the rate performance, leading to a rapid decline on capacity at high current rate (Fig. 8d). On the contrary, it can be seen that the LFP/C-1electrode exhibited small polarization of charge-discharge curves and dramatically improved rate performance. On the basis of above analysis, it can be concluded that vacuum decomposition is beneficial to suppressing particle growth, decreasing particle agglomeration and uniform carbon coating for better electrochemical property of LiFePO4/C composite.

Table 2 depicts the carbon source and rate performance of LiFePO$_4$/C composite synthesized under similar vacuum condition compared with the typical literature data. The LiFePO$_4$/C composite of Ref. 17 shows lower discharge capacities due to its forward work in 2009. Better rate performance of LiFePO$_4$/C composite at 0.2C is observed for Ref. 19, but it required higher sintering temperature

(700 °C) and longer sintering time (12 h). In comparison with Ref. 20 and 21, spherical and uniform particle of this work delivers a slower decline of capacity and superior rate performance at high rates.
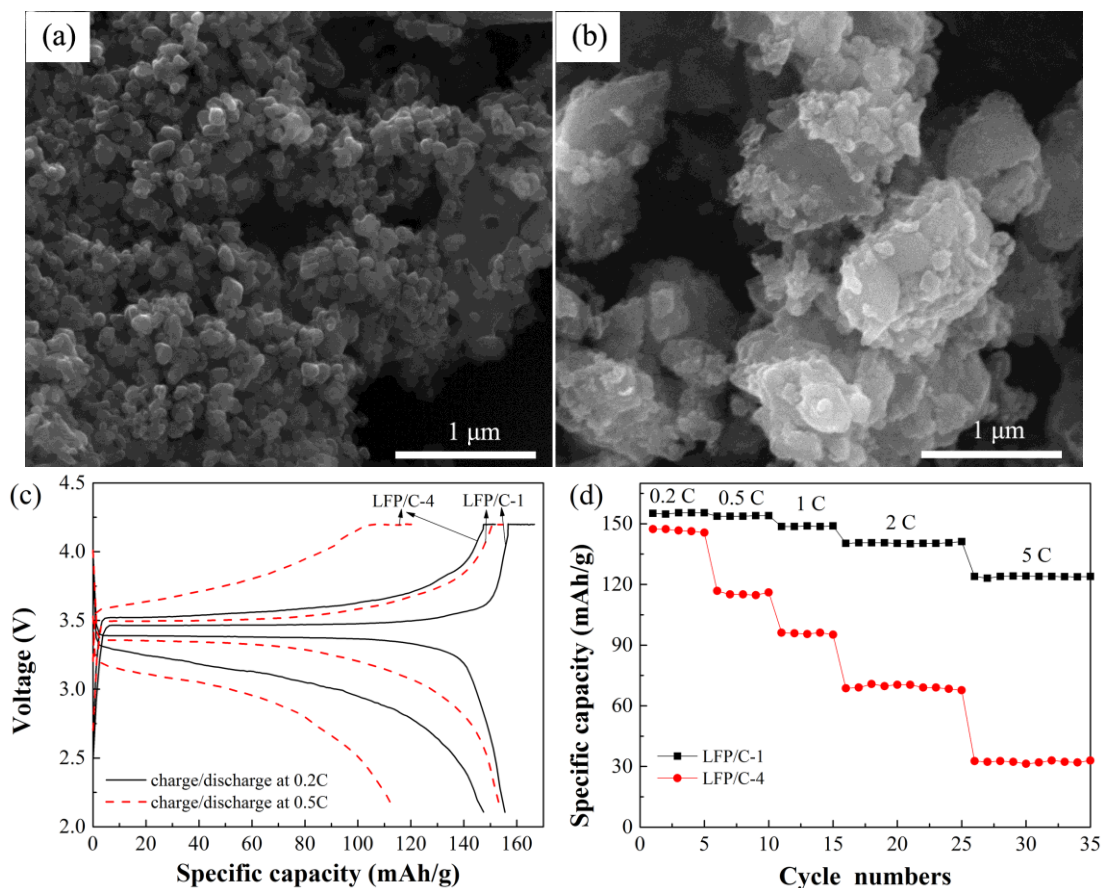
Figure 8. SEM images of (a) LFP/C-1, and (b) LFP/C-4. (c) First charge-discharge profiles for the LFP/C-1and LFP/C-4 electrodes at 0.2C and 0.5C. (d) Comparison of rate capability between LFP/C-1and LFP/C-4 sample (from 0.2C to 5C).

Table 2. Comparison of rate performance for carbon coated LiFePO₄/C composite prepared by different carbon source and synthesis method.

Synthesis method	Carbon source	Rate performance (mAh/g)					Ref.
		0.2C	0.5C	1C	2C	5C	
Vacuum (350 °C,5h) & Vacuum (650 °C,20h)	glucose	138.4	-----	126.8	-----	-----	17
Vacuum (700 °C,12h)	citric acid & starch	160	150	141.1	130.9	105.4	19
Vacuum (350 °C,5h) & Vacuum (650 °C,20h)	glucose	-----	147.5	140	133	117.1 (6C)	20
Vacuum precipitation & Ar (600 °C, 4h)	stearic acid	151	145	140	131(3C)	122	21
Ar (350 °C,4h) & Vacuum (650 °C,6h)	sucrose	155.4	154.0	148.9	140.6	124.1	This work

4. CONCLUSION

In this study, nano-sized $LiFePO_4/C$ composites have been synthesized by precalcination and following vacuum decomposition process for carbon coating. Different carbon resources of sucrose, polyvinyl alcohol (PVA) and citric acid (CA) were used to investigate their pyrolysis behavior on the properties of $LiFePO_4/C$ composite. Results showed that organic carbon decomposed under vacuum condition inhibited grain growth, decreased particle agglomeration and formed uniform particle distribution. Due to the rapid and complete carbonization reaction of carbon under vacuum condition, the $LiFePO_4/C$ composite exhibited a lower carbon content, higher degree of ordered graphitized carbon for better coating structure and conductivity. Compared with PVA and CA, the pyrolysis of sucrose turned to porous architecture during the release of gaseous products. Therefore, the sucrose coated $LiFePO_4/C$ composite showed reduced particle size, regular spherical grains and graphitized carbon coating, resulting in superior overall electrochemical performance of 155.1 and 123.9 mAh/g at 0.2C and 5C rates. For comparison, the sucrose coated $LiFePO_4/C$ composite prepared under traditional argon atmosphere suffered irregular morphology with poor size distribution and serious agglomeration. In summary, carbon coating by vacuum decomposition is conducive to reducing particles size, suppressing the particle agglomeration, and increasing graphitized carbon for $LiFePO_4/C$ composite, resulting in reduced electrode polarization and improved rate performance. Therefore, the carbon coating based vacuum decomposition process is a promising strategy for industrial production of $LiFePO_4/C$ with a higher rate and good cyclic performance.

References

1. P. S. Herle, B. L. Ellis, N. Coombs and L. F. Nazar, *Nat. Mater.*, 3 (2004) 147.
2. A. K. Padhi, K. S. Nanjundaswamy, C. Masquelier, S. Okada and J. B. Goodenough, *J. Electrochem. Soc.,* 144 (1997) 1609.
3. Yamada, S.C. Chung and K. Hinokuna, *J. Electrochem. Soc.*, 148 (2001) A224.
4. B.L. Ellis, W.R.M. Makahnouk, Y. Makimura, K. Toghill and L.F. Nazar, *Nat. Mater.*, 6 (2007) 147.
5. J. H. Hong, Y. F. Wang, G. He and M. Z. He, *Mater. Chem. Phys.*, 133 (2012) 573.
6. N. J. Yun, H. Ha, K. H. Jeong, H. Park and K. Kim, *J. Power Sources,* 160 (2006) 1361.
7. Y. kadoma, J.M. Kim, K. Abiko, K. Ohtsuki, K. Ui, and N. Kumagai, *Elcetrochim. Acta*, 55 (2010) 1034.
8. P. P. Prosini, M. Lisi, D. Zane and M. Pasquali, *Solid State Ionics*, 148 (2002) 45.
9. G. Arnold, J. Garche, R. Hemmer, S. Strobele, C. Vogler and M.Wohlfahrt-Mehrens, *J. Power Sources*, 119 (2003) 247.
10. S. Franger, F. L. Cras, C. Bourbon and H. Rouault, *Electrochem. Solid-State Lett.*, 5 (2002) A231.

11. S. Y. Chung, J. T. Bloking and Y. M. Chiang, *Nat. Mater.*, 1 (2002) 123.
12. X.P. Huang, C. Yang and Y.C. Yao, *Adv. Mater. Res.*, 815 (2013) 423.
13. C.S. Sun, Y. Zhang, X. J. Zhang and Z. Zhou, *J. Power Sources*, 195 (2010) 3680.
14. Z. H. Chen and J. R. Dahn, *J. Electrochem. Soc.*, 149 (2002) A1184.
15. H. Chen, Y.F. Chen, W. Q. Gong, K. X. Xiang, B. Sun and J. H. Liu, *Mater. Lett.*, 65 (2011) 559.
16. B. Huang, X. D. Zheng, X. P. Fan, G. H. Song and M. Lu, *Electrochim. Acta.*, 56 (2011) 4865.
17. J. Huang, L. L. Zhang, G. Peng, S. D. Zhou, J. Guo, H. Y. Wang and X. L. Yang, *J. China Three Gorges. Univ. (Natural Science)*, 31 (2009) 82.
18. F. Liang, Y. C. Yao and Y. N. Dai, *Solid State Ionics*, 214 (2012) 31.
19. Y. X. Guo, X. H. Li, Z. X. Wang and H. Q. Wang, *T. Nonferr. Metal Soc.*, 20 (2010) 1402.
20. L. L. Zhang, G. Peng, X. L. Yang and P. C. Zhang, *Vacuum*, 84 (2010) 1319.
21. J. X. Ren, Y. K. Hu, X. D. Guo, Y. Tang, B. H. Zhong and H. Liu, *Acta Phys. Chim. Sin.*, 30 (2014), 866-872.
22. Y. C Yao, P. W. Qu, X. K. Gan, X. P. Huang, Q. F. Zhao and F. Liang, *Ceram. Int.*, 42 (2016) 18303.
23. L. F. Cheng, G. X. Liang, S. E. Khakani and D. D. MacNeil, *J. Power Sources*, 242 (2013) 656.
24. J. Lim, D. Kim, V. Mathew, D. Ahn, J. Kang, S. W. Kang and J. Kim, *J. Alloys Compd.*, 509 (2011) 8130.
25. S. H. Luo, Z. L. Tang, J. B. Lu and Z. T. Zhang, *Ceram. Int.*, 34 (2008), 1349-1351.
26. J. K. Kim, J. W. Choi, G. S. Chauhan, J. H. Ahn, G. C. Hwang, J. B. Cho and H. J. Ahn, *Electrochim. Acta*, 53 (2008) 8258.
27. M. M. Doeff, Y. Q. Hu, F. Mclarnon and R. Kostrcki, *Electrochem. Solid-State Lett.*, 6 (2003) A207.
28. Z. J. Guo and Z. L. Chen, *J. Electroanal. Chem.*, 754 (2015) 148.
29. R. Trócoli, S. Franger, M. Cruz, J. Morales and J. Santos-Peňa, *Electrochim. Acta*, 135 (2014) 558.
30. X. Xu, Y. L. Xu, H. Zhang, M. D. Ji and H. Dong, *Electrochim. Acta*, 158 (2015) 348.
31. D. Xu, P. F. Wang and B. W. Shen, *Ceram. Int.*, 42 (2016) 5331.
32. C. C. Yang, J. H. Jang, and J. R. Jiang, *Mater. Chem. Phys.*, 165 (2015) 196
33. P. Swain, M. Viji, P. S.V. Mocherla and C. Sudakar, *J. Power Sources*, 293 (2015) 613.
34. L. J. Huang, Y. X. Wang, Z. Huang, J. G. Tang, Y. Wang, J. X. Liu, J. Q. Jiao, J. Q. Liu and A. B. Laurence, *J. Power Sources*, 135 (2014) 558.
35. Z, Jiang and Z. J. Jiang, *J. Alloys Compd.*, 537 (2012) 308.
36. J. Chen, N. Zhao, G. D. Li, F. F. Guo, X. F. Wang, T. K. Jia, J. W. Zhao, Y. G. Zhao, X. L. Wang, and L. Wan, *Mater. Chem. Phys.*, 180 (2016) 244.
37. Y. J. Wang, B. Zhu, Y. M. Wang and F. Wang, *Ceram. Int.*, 42 (2016) 10297.